

# Flux-dependent Kondo temperature in an Aharonov-Bohm interferometer with an in-line quantum dot

Pascal Simon<sup>1,4</sup>, O. Entin-Wohlman<sup>2,3,4,\*</sup> and A. Aharony<sup>2,4,\*</sup>

<sup>1</sup> *Laboratoire de Physique et Modélisation des Milieux Condensés,  
CNRS et Université Joseph Fourier, 38042 Grenoble, France*

<sup>2</sup> *Department of Physics, Ben Gurion University,  
Beer Sheva 84105, Israel*

<sup>3</sup> *Albert Einstein Minerva Center for Theoretical Physics at the Weizmann Institute of Science,  
Rehovot 76100, Israel*

and

<sup>4</sup> *Materials Science Division, Argonne National Laboratory, Argonne, Illinois 60439, USA*

(Dated: May 1, 2019)

An Aharonov-Bohm interferometer (ABI) carrying a quantum dot on one of its arms is analyzed. It is found that the Kondo temperature of the device depends strongly on the magnetic flux penetrating the ring. As a result, mesoscopic finite-size effects appear when the Kondo temperature of the dot on the ABI is significantly smaller than the nominal one of the quantum dot (when not on the interferometer), leading to plateaus in the finite-temperature conductance as function of the flux. The possibility to deduce the transmission phase shift of the quantum dot from measurements of the ABI conductance when it is opened (i.e., is connected to more than two leads) is examined, leading to the conclusion that finite-size effects, when significant, may hinder the detection of the Kondo phase shift.

PACS numbers: 71.10.-w, 72.15.Qm, 73.21.-b, 73.63.Kv

## I. INTRODUCTION

The inherent wave nature of the electron can be revealed in mesoscopic solid-state interferometers. These are built with narrow wave guides for the electronic paths to preserve the coherence of the electron. In general, the Aharonov-Bohm interferometer (ABI) consists of a ring, which is threaded by a Aharonov-Bohm (AB) magnetic flux  $\Phi$ . When the ABI is connected to two reservoirs, via two leads, it is termed ‘closed’, since all the current entering it through one lead leaves it through the other. The ‘open’ ABI connects to additional leads (through which electrons can go astray, so that current is not conserved). The conductance of the interferometer oscillates with the flux, due to interference of the electronic wave function between the two branches of the ring.<sup>1</sup> These AB oscillations of the conductance have been first observed on metallic two-terminal rings (i.e., closed interferometers).<sup>2</sup> Another stringent manifestation of the electronic wave interference is the prediction of a circulating (persistent) current around the interferometer even when the latter is not connected to any reservoir.<sup>3</sup> These theoretical predictions have been tested experimentally by various groups in the last two decades.<sup>4</sup>

Recent experiments have used the ABI, when connected to electronic reservoirs, as a tool to probe quantum coherent transport at the mesoscopic scale. In these experiments, quantum dots are embedded either on one arm<sup>5,6,7,8,9,10</sup> or on both arms<sup>11,12</sup> of the interferometer. These experiments have triggered a large series of theoretical analyses (see Ref. 13 for a review). Transport through a quantum dot can be characterized by a complex transmission amplitude  $t_{QD} = |t_{QD}|e^{i\varphi_{QD}}$ . The AB interferometry promises a way to mea-

sure information on the phase of the quantum dot, for example by measuring the conductance oscillations through an open ABI which obeys certain conditions.<sup>14,15</sup> This information is particularly interesting when the quantum dot is tuned in the Kondo regime, where it mimics the behavior of an artificial magnetic impurity.<sup>8,9,16,17,18</sup> At sufficiently low temperature, this artificial spin-1/2 impurity is screened by the conduction electrons to form a singlet, and then the scattering of the conduction electrons on the impurity is predicted to suffer a  $\pi/2$  phase shift, associated with the so-called unitary limit.<sup>19</sup> A series of recent experiments on open multi-channel solid-state ABI’s<sup>9</sup> have attempted to deduce this Kondo phase shift from the dependence of the conductance oscillations on the dot gate voltage and other parameters. These experimental results were not in agreement with earlier theoretical predictions based on the exact solution of the Anderson model,<sup>20</sup> and consequently several attempts have been made to reconcile theory with the experiment, some questioning the universality of the measured phase.<sup>14,15,21</sup> The theoretical understanding of the experiments in Ref. 9 is still under debate.<sup>22</sup>

Nonetheless, all the recent theoretical analysis of the transport through an ABI containing one or two quantum dots in the Kondo regime<sup>20,23,24,25,26,27,28</sup> ignores the finite-size extension of the so-called Kondo cloud. Finite-size effects occur for example when the (artificial) magnetic impurity is embedded into some finite-size box.<sup>29</sup> Theoretical predictions indicate that these finite-size effects may affect the screening of an artificial impurity embedded in an isolated ring (i.e., not connected to any external leads).<sup>30</sup> It has indeed been proposed that persistent currents in such a ring containing a quantum dot may offer a way to probe directly this large Kondo length scale.<sup>30</sup> (See also Refs. 31,32,33,34,35,36.) When the Kondo screening cloud becomes of order of the ring size or larger,

Ref. 30 found a crossover in the flux-dependence of the persistent current, from a (large amplitude) saw tooth shape to a (small amplitude) sinusoidal shape. Unfortunately, persistent current experiments are generally delicate and very sensitive to disorder.

However, one may wonder what would be the signature of the finite-size extension of the Kondo cloud when the ABI ring is connected to several reservoirs. A priori, the physics is different because the artificial impurity is now coupled to a continuum and one may expect these finite-size effects to vanish. In fact, this is not always the case, particularly when the quantum dot is coupled to a finite-size mesoscopic wire, which is itself weakly coupled to a reservoir.<sup>37,38</sup> It has been shown that when the wire level spacing  $\Delta_r$  is larger than the reference Kondo temperature  $T_K^0$  of a quantum dot directly coupled to infinite leads, finite-size effects do occur. The main consequence is a strong renormalization of the genuine Kondo temperature of the artificial impurity,  $T_K$ , and a strong dependence of  $T_K$  on the local density of states seen by the artificial impurity.<sup>37</sup> In this paper we therefore analyze the transport properties of an ABI weakly coupled to reservoirs and containing an in-line quantum dot tuned to be in the Kondo regime. In particular we show that the Kondo temperature strongly depends on the AB phase, leading to some direct consequences on the finite temperature conductance through the ABI. (For a discussion of the fluctuations of the Kondo temperature as function of the magnetic flux in a chaotic ABI, see Ref. 39.)

The plan of the paper is the following: In section II, we

describe our model Hamiltonian for the closed ABI and analyze how finite-size effects affect the Kondo temperature. We especially show that the Kondo temperature acquires a strong dependence on the AB phase in a one-dimensional description of the ABI. In section III, we present our results for the conductance through the closed ABI using the slave-boson mean-field theory approximation scheme. In Sec. IV we analyze the Kondo temperature and the conductance of an open interferometer, by modifying our model to include numerous additional leads. Finally, section V contains a discussion of our results and our conclusions. An appendix details the calculation of the conductance through the ABI containing an interacting quantum dot.

## II. ENERGY SCALES IN AN AB INTERFEROMETER

### A. Model Hamiltonian

In order to analyze the role played by finite-size effects in an ABI, we consider the simple one-dimensional model depicted in Fig. 1. The tight-binding Hamiltonian describing the ABI shown in that figure reads

$$H = H_L + H_I + H_D + H_{L,I} + H_{I,D}, \quad (1)$$

where the subscripts  $L$ ,  $I$ , and  $D$  stand for the leads, the interferometer, and the dot, respectively.

In Eq. (1),

$$H_L = -J \left[ \sum_{i=-\infty}^{-n_l-2} + \sum_{i=n_r+1}^{\infty} \right] \sum_{\sigma} (c_{i\sigma}^{\dagger} c_{i+1\sigma} + h.c.), \quad (2)$$

is the lead Hamiltonian, and

$$H_I = -J \sum_{i=-n_l}^{-2} \sum_{\sigma} (c_{i\sigma}^{\dagger} c_{i+1\sigma} + h.c.) + \epsilon_l \sum_{i=-n_l}^{-1} \sum_{\sigma} n_{i\sigma} - J \sum_{i=1}^{n_r-1} \sum_{\sigma} (c_{i\sigma}^{\dagger} c_{i+1\sigma} + h.c.) + \epsilon_r \sum_{i=1}^{n_r} \sum_{\sigma} n_{i\sigma} - J \sum_{i=-l_0-1}^{l_0} \sum_{\sigma} (a_{i\sigma}^{\dagger} a_{i+1\sigma} + h.c.) + \epsilon_0 \sum_{i=-l_0}^{l_0} \sum_{\sigma} a_{i\sigma}^{\dagger} a_{i\sigma}, \quad (3)$$

describes the ring, with  $n_{i\sigma} = c_{i\sigma}^{\dagger} c_{i\sigma}$ . The upper left and right branches of the ABI contain  $n_l$  and  $n_r$  sites, respectively, and the lower arm contains  $n_0 = 2l_0 + 1$  sites. In Eqs. (2) and (3),  $c_{i\sigma}^{\dagger}$  creates an electron with spin  $\sigma = \uparrow, \downarrow$  on site  $i$  either in the upper branch of the ABI (for  $i \in [-n_l, n_r]$ ) or in the leads ( $i < -n_l$  and  $i > n_r$ ), whereas  $a_{i\sigma}^{\dagger}$  with  $i \in [-l_0, l_0]$  creates an electron in the lower part of the ABI. (We use a different labelling in order to distinguish electrons on the upper branch from those on the lower branch.) We assign different sites energies,  $\epsilon_l$ ,  $\epsilon_r$ , and  $\epsilon_0$  on these three respective branches. We also identify  $a_{-l_0-1} \equiv c_{-n_l} \equiv c_a$  and  $a_{l_0+1} \equiv c_{n_r} \equiv c_b$  (all with spin  $\sigma$ ) for the sites connecting the ring to the leads. The Hamiltonian of the quantum dot is

$$H_D = \epsilon_d \sum_{\sigma} n_{d\sigma} + U n_{d\uparrow} n_{d\downarrow}. \quad (4)$$

In most of our calculations we assume that the Coulomb energy  $U$  is larger than all other energies in the problem, and thus take the limit  $U \rightarrow \infty$ . Also,

$$H_{L,I} = - \sum_{\sigma} (J_L c_{-n_l-1\sigma}^{\dagger} c_{-n_l\sigma} + J_R c_{n_r\sigma}^{\dagger} c_{n_r+1\sigma} + h.c.),$$

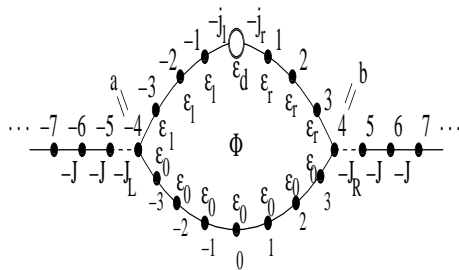


FIG. 1: Our model for the ABI with  $n_l = n_r = 4$ ,  $n_0 = 2l_0 + 1 = 7$ . The extremities of the interferometer are denoted by  $a$  and  $b$ . Here  $a$  and  $b$  correspond respectively to points  $-4$  and  $+4$ .

$$H_{I,D} = -e^{-i\alpha/2} \sum_{\sigma} (j_l c_{-1\sigma}^{\dagger} c_{d\sigma} + j_r c_{d\sigma}^{\dagger} c_{1\sigma}) + h.c., \quad (5)$$

describe the coupling of the ring to the leads and to the dot. The interferometer depicted in Fig. 1 is threaded by a magnetic field. This gives rise to the phase factors appearing in Eqs. (5), with  $\alpha = 2\pi\Phi/\Phi_0$ , where  $\Phi$  is the total magnetic flux penetrating the ABI ring and  $\Phi_0$  is the flux quantum. Using gauge invariance, we have distributed this phase on the tunneling amplitudes between the dot and the ring. The total number of sites on the interferometer,  $L = n_l + n_r + n_0$ , determines the size of the ring.

In the following we will be interested in the regime where the quantum dot describes the behavior of an artificial magnetic impurity in the Kondo regime, i.e., when  $n_d \equiv n_{d\uparrow} + n_{d\downarrow} \sim 1$ . The important energy scale of the problem is then the Kondo temperature  $T_K$ . The next section is devoted to an analysis of this energy scale.

## B. The Kondo temperature

When the ring is disconnected from the reservoirs, it has been shown in Ref. 30 that the ring circumference  $L$  introduces a cutoff energy  $\Delta_r = \hbar v_F/L$  (where  $v_F$  denotes the Fermi velocity of the conduction electrons), which replaces the temperature  $T$  in the renormalization of the Kondo coupling when  $T < \Delta_r$ , hence preventing a perfect screening of the impurity. The situation becomes more delicate when finite-size effects (brought about by the finite length of the ring) combine with the coupling to the continuum (described by the leads). In Ref. 37, a setup in which a quantum dot is connected to finite-size wires which are in turn weakly coupled to reservoirs has been analyzed. Then, the dot non-interacting self-energy, and in particular the local density of states (LDOS) on the dot, become structured in energy due to the finite-size effects. As a result, the Kondo temperature depends on the fine structure of the LDOS.

In the present configuration, the finite-size ring is coupled to the continuum, and in addition is threaded by a magnetic flux. Indeed, we find below that the Kondo temperature varies strongly (over several decades) with the magnetic flux when the ring energy spacing  $\Delta_r$  is larger than the bare Kondo temperature  $T_K^0$ , or equivalently, when the ring length  $L = \hbar v_F/\Delta_r$  is smaller than the Kondo length scale,  $\xi_K^0 \equiv \hbar v_F/T_K^0$ . In fact, such a result can be expected, at least qualitatively, as can be understood by considering special cases: In the limit where the ABI becomes disconnected from the leads, we should recover the isolated ring case studied in Ref. 30, where finite-size effects were shown to appear when  $T_K^0 \ll \Delta_r$ . Another particularly interesting case is a symmetric (under parity) ABI with only a single site, 0, on the lower branch, and  $n_l = n_r$  (in the notations used above). In this

specific case, it is convenient to perform a folding even/odd transformation by defining  $c_i^{e/o} = (c_i \pm c_{-i})/\sqrt{2}$ ,  $\forall i > 0$ . In the new basis, the quantum dot is coupled to two finite-size wires, of respective lengths  $n_l + 1$  and  $n_l$ , which are coupled to a continuum via their other extremity. The AB phase enters only through the tunnel amplitudes between the even/odd finite-size wires and the dot: The corresponding matrix elements are  $j_l \sqrt{2} \cos(\alpha/2)$  for the even part and  $i j_l \sqrt{2} \sin(\alpha/2)$  for the odd part.<sup>40</sup> Such a situation was already studied in Ref. 37, where it was shown that finite-size effects only occurs for  $n_l \lesssim \xi_K^0$ .

On the other hand, when the ring size is very large compared to the Kondo length scale, finite-size effects are washed out. For example, in the second particular case discussed in the previous paragraph, it is easy to see that in the large-size ABI the Kondo temperature is essentially flux-independent.<sup>40</sup> On a more general footing, one may give the following heuristic argument: The Kondo screening cloud is localized in the upper branch of the ABI around the quantum dot. The AB phase can be assigned, by a gauge transformation, to the lower branch alone. Then, electrons participating in the dynamical screening of the impurity will not “see” the AB phase. In such a situation we expect the associated Kondo temperature to be the bare Kondo temperature  $T_K^0$ .

From the aforementioned general arguments, one may therefore expect that the Kondo temperature in an ABI will be affected both by the finite size of the ABI branches and by the magnetic flux. The Kondo temperature is the energy scale separating the high temperature perturbative regime, where the impurity is weakly screened, from the low temperature strong-coupling regime, where it forms a singlet with the conduction electrons. Since it is a crossover scale, there are many ways to define it, all capturing the correct order of magnitude. In

this paper, we mainly use two definitions, one resulting from the slave-boson mean-field theory (see Sec. III A), which expresses the Kondo temperature in terms of the parameters of the non-interacting system (when there are no interactions on the dot) and another one resulting from the renormalization group approach.

The non-interacting Green function on the dot can be written as

$$G_{dd}^0 = [\omega - \epsilon_d - \Sigma_{dd}^0(\omega)]^{-1}, \quad (6)$$

where

$$\Sigma_{dd}^0(\omega) = \delta\epsilon(\omega) - i\Delta(\omega) \quad (7)$$

is the dot non-interacting self-energy, and  $\epsilon_d$  is the single-particle on-site energy on the dot [see Eq. (4)]. For large  $U$ , the two parts of the non-interacting self-energy determine *a priori* the Kondo temperature. When the self-energy is a smooth function around the Fermi energy,  $E_F$ , one obtains the standard analytical expression for the Kondo temperature,

$$T_K \approx D_0 \exp\left(\pi \frac{\epsilon_d - \delta\epsilon(E_F)}{2\Delta(E_F)}\right), \quad (8)$$

where  $D_0$  denotes the half-bandwidth on the leads. On the other hand, when the self-energy varies abruptly around the Fermi energy (which is typically the case for the ABI), one needs to solve numerically the self-consistent slave boson mean-field integral equations in order to find that temperature. Denoting the Kondo temperature of this situation by  $T_K^{\text{SBMFT}}$ , one has

$$T_K^{\text{SBMFT}} \approx b_0^2 \Delta(E_F), \quad (9)$$

where  $b_0$  is the slave boson parameter (see Sec. III A).

Since the self-energy given in Eq. (7) pertains to a non-interacting system, it can be calculated in a straightforward way. In the case of the Hamiltonian Eq. (1) (see also Fig. 1), it can be expressed as

$$\Sigma_{dd}^0(\omega) = j_l^2 g_{-1-1}(\omega) + j_r^2 g_{11}(\omega) + 2j_l j_r \cos \alpha g_{-11}(\omega), \quad (10)$$

where  $g_{ij}(\omega)$  are the Green functions of the system without the quantum dot (i.e., for  $j_l = j_r = 0$ ), and therefore refer to a non-interacting system. Note that these Green functions *do not* depend on the AB flux, so that the entire flux dependence of the non-interacting self-energy comes from the interference term in Eq. (10). This dependence makes both  $T_K$  and  $T_K^{\text{SBMFT}}$  flux-dependent as well.

To ensure that this dependence is not a result of our definition of the Kondo temperature, we have also computed the Kondo temperature as defined by the renormalization group (RG) technique,  $T_K^{\text{RG}}$ ,<sup>37,41</sup>

$$\left[ \int_{-D_0}^{-T_K^{\text{RG}}} + \int_{T_K^{\text{RG}}}^{D_0} \right] d\omega \frac{J_K \rho(\omega)}{2|\omega|} = 1, \quad (11)$$

where  $J_K$  is the Kondo coupling and  $\rho(\omega)$  is the non-interacting local density of states (LDOS) on the dot, given in our model by  $\Delta(\omega)/(j_l^2 + j_r^2)$ . In the  $U \rightarrow \infty$  limit of the Anderson description of the quantum dot,  $J_K = 2(j_l^2 + j_r^2)/|\epsilon_d|$ . It is worth noting that when a quantum dot (in the Kondo regime) is connected to two large reservoirs,  $\rho(\omega) \sim \rho(E_F)$ , and therefore  $T_K^{\text{RG}} = D_0 \exp[-1/(J_K \rho(E_F))] = D_0 \exp(\pi \epsilon_d / 2\Delta(E_F))$ , which agrees with Eq. (8) ( $\delta\epsilon(E_F) \sim 0$  in this case).

We exemplify the AB phase dependence of the Kondo temperature below, utilizing two different parameterizations of the ABI.

### 1. The Kondo temperature of a dot embedded in a mesoscopic ABI ring

As explained above, the quantity which determines the Kondo temperature in the large- $U$  limit is the non-interacting self-energy of the dot. Its calculation requires the Green functions of the system without the dot. (Our Green functions are the retarded ones, unless specified explicitly otherwise.) One may present those as a matrix of dimension  $(L \times L)$  where  $L = n_l + n_r + n_0$  is the total number of sites on the interferometer, with the dot excluded,

$$\hat{g} = [\omega \hat{I} - \hat{H} - \hat{\Sigma}]^{-1}. \quad (12)$$

Here  $\hat{\Sigma}$  is the self-energy due to the two (or more) semi-infinite leads. In our model,  $\hat{\Sigma}$  has just two non-zero matrix elements,  $\hat{\Sigma}_{aa}$  and  $\hat{\Sigma}_{bb}$ , see Fig. 1. Once the matrix of Eq. (12) is inverted, the result is used in Eq. (10) to yield the dot self-energy. Generally, this scheme is numerically quite time consuming since for each frequency  $\omega$  one needs to invert an  $L \times L$  matrix. To overcome this difficulty we utilize below an approximate solution for a general ring, which exemplifies the mesoscopic finite-size effects. We then present an analytic derivation for a very small model system where the ring contains a single site besides the dot. Even this small ring, when weakly coupled to the leads, already captures the strong dependence of the Kondo temperature on the AB flux. However, such a small model is insufficient to describe properly mesoscopic finite-size effects.

In the limit where the ABI is weakly-coupled to the leads (i.e., when  $J_L^2, J_R^2 \ll J^2$ ) and for  $\epsilon_0 = \epsilon_l = \epsilon_r$ , one can obtain a rather good approximation for the non-interacting Green functions by approximating the local density of states in the ring by a Lorentzian. This approximation has been successfully used previously in Ref. 37. In this approximation, the Green function  $g_{mn}$ , where  $m$  and  $n$  are two sites on the ring, is given by

$$g_{mn} \approx \frac{2}{L+1} \sum_{j=1}^L \frac{\sin(q_r j m) \sin(q_r j n)}{\omega - \epsilon_j - \delta\epsilon_j + i\Delta_j}, \quad (13)$$

where the variables  $q$  and  $\omega$  are related to one another by  $\omega = -2J \cos(q)$  (here and below we measure lengths in units of the lattice constant). In Eq. (13),

$$\epsilon_j = -2J \cos(q_r j) + \epsilon_r, \quad (14)$$

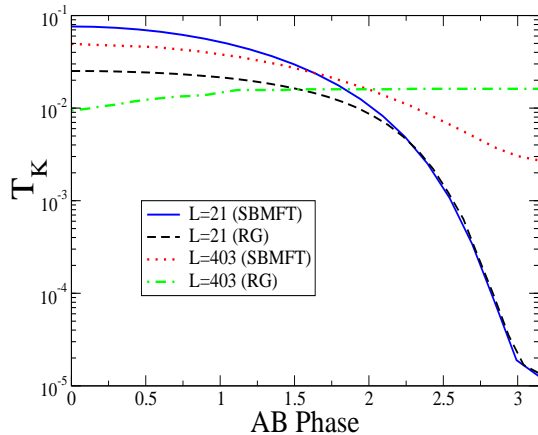


FIG. 2: Kondo temperatures as function of the AB phase  $\alpha = 2\pi\Phi/\Phi_0 \in [0, \pi]$  calculated using either the SBMFT definition, Eq. (9), or the RG definition, Eq. (11), for two different ABI sizes:  $L = 21$  (the full and long dashed lines) and  $L = 403$  (the dotted and dashed-dotted lines). The following parameters are used:  $j_l = j_r = 0.35$ ,  $\epsilon_d = -0.7$  (giving  $T_K^0 \sim 0.011$  or  $\xi_K^0 \sim 180$ ) and  $J_L = J_R = 0.6$ ,  $\epsilon_l = \epsilon_r = \epsilon_0 = 0$ .

with

$$q_{rj} = \frac{\pi j}{L+1}; \quad j = 1, \dots, L. \quad (15)$$

For the case of two leads only,  $\delta\epsilon_j$  and  $\Delta_j$  are given by

$$\begin{aligned} \delta\epsilon_j &= -\frac{2}{L+1} \left( \frac{J_L^2}{J} \sin^2(q_{rj}n_l) \sin(q) \right. \\ &\quad \left. + \frac{J_R^2}{J} \sin^2(q_{rj}n_r) \sin(q) \right), \\ \Delta_j &= \frac{2}{L+1} \left( \frac{J_L^2}{J} \sin^2(q_{rj}n_l) \cos(q) \right. \\ &\quad \left. + \frac{J_R^2}{J} \sin^2(q_{rj}n_r) \cos(q) \right). \end{aligned} \quad (16)$$

We have used the approximate expression (13) for the non-interacting Green functions, in conjunction with Eq. (9), to compute numerically the dependence of the Kondo temperature,  $T_K^{SBMFT}$ , on the AB phase. Using  $n_l = n_r = 5$ , and  $n_0 = 11$ , which yield for the total size of the ring  $L = n_l + n_r + n_0 = 21$ , one finds that the Kondo temperature varies over at least three decades (the continuous line in Fig. 2). (The energy units are set by the tight-binding amplitude on the leads,  $J = 1$ .) This huge variation is not an artifact of our definition of the Kondo temperature (resulting from the slave-boson technique). Using the renormalization-group definition, Eq. (11), we obtain, for the same parameters, the long-dashed line in Fig. 2. Clearly, both definitions give almost the same huge variation (differing around  $\alpha = 0$  by a factor which is less than 3).

On the other hand, at larger ring sizes, the variations of the Kondo temperature with the flux are strongly suppressed, as is seen in Fig. 2. We note that the RG definition predicts a Kondo temperature which is almost phase-independent (it varies by just a factor 2), whereas the SBMFT definition predicts a variation by one decade. The reason for this difference stems from the fact that the integral appearing in the RG definition averages over the energy variations of the density of states, making  $T_K^{RG}$  less sensitive as compared to  $T_K^{SBMFT}$ .<sup>42</sup> Nevertheless, the variations of  $T_K$  of the  $L = 403$  ring are overall  $\sim 3$  orders of magnitude smaller than those of the  $L = 21$  one, proving that finite-size effects are prominent for  $L \lesssim \xi_K^0$ . This strong modulation of the Kondo temperature with the magnetic flux for small ABI's will clearly affect the thermodynamic and transport properties of a mesoscopic ring.

## 2. The Kondo temperature of a smaller configuration

When the ring is very small, such that it contains a single site in addition to the dot, it is possible to find a simple analytical expression for the non-interacting self-energy. Such a system has been studied in Ref. 26. In our parametrization, it corresponds to a quantum dot directly connected to the leads, and interfering with a lower path characterized by a single energy level  $\epsilon_0$  connected again directly to the leads with hopping amplitudes  $i_\ell$  and  $i_r$  for the left and right leads, respectively. This model system still demonstrates the remarkable variation of the Kondo temperature with the AB phase.

In this model system the non-interacting dot self-energy is

$$\Sigma_{dd}^0(\omega) = g_L(\omega)(j_\ell^2 + j_r^2 + g_L^0(\omega)g_{00}(\omega)|Y|^2). \quad (17)$$

Here,  $g_L$  reflects the effect of the one-dimensional leads,

$$g_L(\omega) = \frac{2}{N} \sum_k \frac{\sin^2 k}{\omega - \epsilon_k} = -\frac{e^{iq}}{J}, \quad (18)$$

$g_{00}$  is the Green function of the lower arm of the interferometer, when disconnected from the dot,

$$g_{00}(\omega) = \frac{1}{\omega - \epsilon_0 - g_L(\omega)(i_\ell^2 + i_r^2)}, \quad (19)$$

and

$$|Y|^2 = j_\ell^2 i_\ell^2 + j_r^2 i_r^2 + 2j_\ell j_r i_\ell i_r \cos \alpha, \quad (20)$$

containing the dependence of the self-energy on the AB flux.

To use these results in the expression for the Kondo temperature, Eq. (8), we take the Fermi energy to be in the middle of the energy bands of the leads, i.e.,  $\omega = 0$  and  $q = \pi/2$ . Then

$$g_{00}(E_F) = \frac{1}{-\epsilon_0 + i \frac{i_\ell^2 + i_r^2}{J}}. \quad (21)$$

For a symmetric configuration,  $i_\ell = i_r$  and  $j_\ell = j_r$ , the self-energy at zero frequency can be written in terms of the

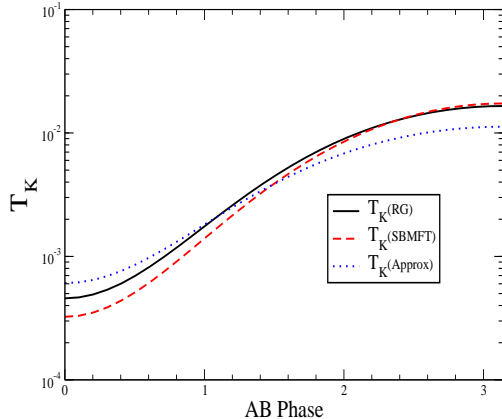


FIG. 3: The Kondo temperature as function of the AB phase,  $\alpha = 2\pi\Phi/\Phi_0 \in [0, \pi]$ , for the small configuration described in Sec. II B 2. The parameters used are :  $T_B = 0.5$ ,  $\epsilon_d = -0.7$ ,  $\epsilon_l = \epsilon_r = \epsilon_0 = -1$  and  $j_l = j_r = 0.35$ .

transmission ( $T_B = 4(i_\ell^2/J)^2/[\epsilon_0^2 + 4(i_\ell^2/J)^2]$ ) and reflection ( $R_B = 1 - T_B$ ) of the lower arm of the ring, yielding

$$\begin{aligned} \Delta(E_F) &= 2\frac{j_\ell^2}{J}(1 - T_B \cos^2 \frac{\alpha}{2}), \\ \delta\epsilon(E_F) &= \text{sgn}(\epsilon_0)2\frac{j_\ell^2}{J}\sqrt{R_B T_B} \cos^2 \frac{\alpha}{2}. \end{aligned} \quad (22)$$

The dependence of the Kondo temperature on the AB phase, calculated for this model using either the RG definition, Eq. (11), or the SBMFT definition, Eq. (9), or the approximate definition, Eq. (8), is depicted in Fig. 3. It is seen that even for this minimal geometry, the Kondo temperature varies by a factor  $\sim 50$ . By taking smaller values of the dot tunneling amplitudes, this factor can be even further enhanced by several orders of magnitude.

### III. THE CONDUCTANCE THROUGH THE ABI

#### A. The slave-boson mean-field theory

In order to study the finite temperature transport through the ABI, we need a reliable approximation scheme that will describe well the electronic correlations on the dot localized level on one hand, and will be sufficiently easy to handle on the other. Since the conductance through the ABI can be expressed in terms of the dot Green function, an appropriate approximation scheme should be applied to this entity. We choose to employ the slave-boson mean-field theory (SBMFT). This technique is known to capture qualitatively the low-temperature properties of the Anderson model, and in particular it provides a correct estimate of the Kondo temperature, as discussed above.

For the application of the slave-boson technique to the ABI, it is useful to re-write the model Hamiltonian Eq. (1) in a way that singles out the parts which contain the dot operators. This is accomplished by writing

$$H = H_D + H_{tun} + H_{net}, \quad (23)$$

where  $H_D$  is the dot Hamiltonian, given in Eq. (4),  $H_{tun}$  describes the coupling between the dot and the ABI and is given by the second equation of (5), and  $H_{net}$  contains all other parts of the Hamiltonian (which are non-interacting).

The slave-boson technique is usually applied<sup>41</sup> in the case where the Hubbard  $U$  is the largest energy of the problem. In practice, we set  $U = \infty$ . In that limit, the creation operator on the quantum dot can be written as  $c_{d\sigma}^\dagger = f_\sigma^\dagger b$ , where the fermionic operator  $f_\sigma^\dagger$  creates a singly occupied state on the dot, while the bosonic operator  $b$  creates an empty state (i.e., a two-hole state) there. Since  $U = \infty$ , the dot can be at most singly occupied, and therefore one must impose the constraint

$$b^\dagger b + \sum_\sigma f_\sigma^\dagger f_\sigma = 1. \quad (24)$$

In the mean-field treatment of the slave-boson technique, the boson operator  $b$  is replaced by a c-number,  $b_0$ , and the constraint (24) is implemented by introducing the Lagrange multiplier  $\lambda_0$ . In this way, the Hamiltonian becomes a non-interacting one, and is consequently easy to solve. However, the parameters  $b_0$  and  $\lambda_0$  have to be solved self-consistently.

Applying the SBMFT to our model Hamiltonian Eq. (23), we find that the part referring to the dot alone changes into

$$H_D \rightarrow \epsilon_f \sum_\sigma f_\sigma^\dagger f_\sigma + \lambda_0(b_0^2 - 1), \quad (25)$$

where we have defined  $\epsilon_f = \epsilon_d + \lambda_0$ , and  $H_{tun}$  changes into

$$H_{tun} = -e^{-i\alpha/2} b_0 \sum_\sigma (j_\ell c_{-1\sigma}^\dagger f_\sigma + j_r f_\sigma^\dagger c_{1\sigma}) + h.c. \quad (26)$$

The values of  $\lambda_0$  and  $b_0$  are determined by minimizing the free energy of the system, defined by  $F_{MF} = -\frac{1}{\beta} \log Z + \lambda_0(b_0^2 - 1)$ , where  $Z$  is the partition function. The mean-field free energy is conveniently expressed in the form

$$F_{MF} = -\frac{2}{\pi} \int_{-D_0}^{D_0} d\omega f(\omega) \text{Im}[\ln G_f^R(\omega)] + \lambda_0(b_0^2 - 1), \quad (27)$$

where  $f(\omega) = 1/[1 + \exp(\beta\omega)]$  is the Fermi function, and  $G_f^R$  is the retarded Green function on the dot. Since the mean-field Hamiltonian is non-interacting, this retarded Green function is given by

$$G_f^R(\omega) = [\omega + i\eta - \epsilon_f - \Sigma_f^R(\omega)]^{-1}, \quad (28)$$

with  $\Sigma_f^R(\omega) = \delta\epsilon_f(\omega) - i\Delta_f(\omega)$  being the dot self-energy associated with the SBMFT, Eqs. (25) and (26). This self-energy, in turn, is given by our original non-interacting self-energy, [see Eq. (6)]  $\Sigma_f^R(\omega) = b_0^2 \Sigma_{dd}^{0R}(\omega) = b_0^2 [\delta\epsilon(\omega) - i\Delta(\omega)]$ , where  $\Sigma_{dd}^{0R}(\omega)$  does not depend on  $b_0$ .

Inserting Eq. (28) into Eq. (27), the mean-field free energy becomes

$$F_{MF} = \frac{2}{\pi} \int_{-D_0}^{D_0} d\omega f(\omega) \arctan \left( \frac{b_0^2 \Delta(\omega)}{\omega - \epsilon_f - b_0^2 \delta\epsilon(\omega)} \right) + (\epsilon_f - \epsilon_d)(b_0^2 - 1). \quad (29)$$

Minimizing it with respect to the parameters  $b_0$  and  $\epsilon_f$  (which replaces the parameter  $\lambda_0$ ), leads to a set of two coupled integral equations,

$$\begin{aligned} \frac{2}{\pi} \int_{-D_0}^{D_0} d\omega f(\omega) \frac{\Delta_f(\omega)}{[\omega - \epsilon_f - \delta\epsilon_f(\omega)]^2 + \Delta_f^2(\omega)} \\ + b_0^2 - 1 = 0, \\ \frac{2}{\pi} \int_{-D_0}^{D_0} d\omega f(\omega) \frac{\Delta(\omega)(\omega - \epsilon_f)}{[\omega - \epsilon_f - \delta\epsilon_f(\omega)]^2 + \Delta_f^2(\omega)} \\ + (\epsilon_f - \epsilon_d) = 0. \end{aligned} \quad (30)$$

In the simplest case in which the self-energy is independent of the frequency,  $\delta\epsilon_f(\omega) \rightarrow b_0^2 \delta\epsilon$  and  $\Delta_f(\omega) \rightarrow b_0^2 \Delta$ , these two equations can be solved in a straightforward manner at zero temperature.<sup>41</sup> In the general case they must be solved numerically by an iteration procedure, as function of the temperature. In this way one obtains the dot Green function, which is used below in the calculation of the conductance.

### B. SBMFT results for the conductance of a weakly-coupled closed ABI

A general expression for the finite temperature conductance through the ABI can be derived as function of the exact retarded Green function on the dot and the ABI parameters. This expression is derived in the Appendix. However, it is worth noting that since in the SBMFT the Green function on the dot is that of a non-interacting system, the resulting expression is equivalent to that derived from the Landauer-like formula,<sup>43</sup>

$$G = \frac{2e^2}{h} \int d\omega \frac{4J_L^2 J_R^2 (1 - \frac{\omega^2}{4J^2})}{J^2} \left( \frac{-\partial f}{\partial \omega} \right) |G_{ab}^R|^2, \quad (31)$$

where  $G_{ab}^R$  is the exact retarded Green function for the sites  $a$  and  $b$ .

Using the expression (31), we have calculated the conductance as function of  $\alpha \in [0, \pi]$  for several temperatures, using parameters as in section II B,  $j_l = j_r = 0.35$ ,  $\epsilon_d = -0.7$ ,  $J_L = J_R = 0.6$ ,  $n_l = n_r = 5$ ,  $n_0 = 11$ , and  $\epsilon_l = \epsilon_r = \epsilon_0 = 0$ . These calculations have been performed employing the approximation of weakly coupled leads, as summarized by Eqs. (13)-(16). The results are depicted in Fig. 4: The upper panel pertains to the situation in which the quantum dot is in the Kondo regime, and the lower panel is for a non-interacting quantum dot at resonance. Note that the conductance is an even function of the AB phase  $\alpha$  and has a  $2\pi$  periodicity.

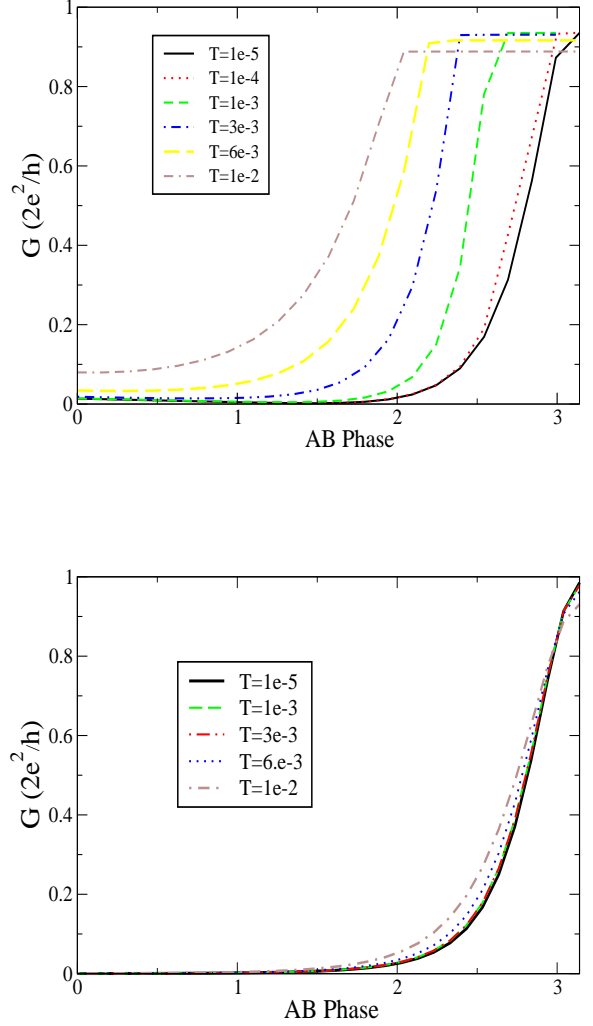


FIG. 4: The conductance as function of the AB phase,  $\alpha = 2\pi\Phi/\Phi_0$ , for various values of the temperature. The upper panel shows the conductance when the dot is in the Kondo regime, and the lower panel shows it for a non-interacting quantum dot at resonance.

When the temperature is below the Kondo temperature  $T_K(\alpha)$ , for any value of the AB phase  $\alpha$ , the spin of the artificial impurity is almost fully screened. This situation corresponds to the unitary limit of the conductance. In this temperature regime, the quantum dot is perfectly transmitting and can be effectively replaced by a non-interacting quantum dot at resonance. Indeed, the conductances displayed in the upper and lower panels of Fig. 4 are comparable for  $T = 10^{-5}$ . However, when the temperature becomes of order of the Kondo temperature or larger, the transmission of the interacting dot is strongly suppressed. Therefore, transport through the ABI is essentially carried via the lower branch, and we thus expect the conductance to be flux independent. Due to the huge variation of the Kondo temperature with the AB phase  $\alpha$ , the interesting situation occurs

when  $\min[T_K(\alpha)] \ll T \ll \max[T_K(\alpha)]$ . In this temperature regime, there are domains of  $\alpha$  in which the dot transmission is very small; these are associated with plateaus of a large conductance through the ABI. This is illustrated in the upper panel of Fig. 4, where such plateaus appear around  $\alpha = \pi$  (for our choice of parameters, this regime corresponds to the lowest Kondo temperature) and become larger as we increase the temperature. The more we increase the temperature, the more dramatic this effect is. Strictly speaking, when the temperature is increased beyond the Kondo temperature, the SBMFT approximation loses its validity. Nevertheless, we believe that the main effect, i.e., the strong decrease of the dot transmission, is qualitatively captured. It seems plausible that within a more numerically-accurate approach like the numerical renormalization group (NRG), the conductance curves will be smoothed, such that there will be a weak phase dependence in the plateau regime. Such a weak dependence cannot be captured by the present method.

In order to highlight that these features are associated with interaction effects, we also plot the conductance at the same temperatures for a non-interacting quantum dot (see the lower panel of Fig. 4). The curves are very similar to the ones in the upper panel of Fig. 4 when the temperature is much smaller than the (minimal) Kondo temperature, but differ drastically at some intermediate temperature. The fact that the conductance does not completely reach the unitary limit even for the non-interacting situation is due to the approximations [Eqs. (13)-(16)] used in calculating the non-interacting Green functions. This inability to reach the unitary limit is actually enhanced by the SBMFT approximation for the interacting case (see the upper panel of Fig. 4). Nevertheless, the main features which we describe are qualitatively well reproduced.

The qualitative features of the results depicted in Fig. 4 do not depend on our particular choice of the parameters. They reflect the strong modulation of the Kondo temperature with the flux, and are associated mainly with the finite size of the ring. In order to further exemplify this point we have calculated the variation of the conductance at different temperatures for a large-size ABI, having  $L = 403 > \xi_K^0$ . The results are depicted in Fig. 5. At this large size the slave-boson parameters,  $b_0$  and  $\epsilon_f$ , are almost independent of the AB flux, eliminating effectively the flux-dependence of the interaction effects. Then, the flux dependence of the ABI properties arise simply from the flux dependence of the non-interacting self-energy.<sup>42</sup> As a result, the conductance no longer displays the plateau-like features that appeared for the small-size ABI. It is only at high temperatures,  $T \geq 6 \cdot 10^{-3}$ , that the conductance appears flatter almost over the entire flux range. The conductance curves in Fig. 5 can be well interpreted by a Kondo temperature which is almost independent of the flux (as corroborated by Fig. 2). At temperatures higher than the Kondo one, the transmission through the dot becomes small, independently of the AB flux, and the conductance is mainly through the lower arm of the interferometer.

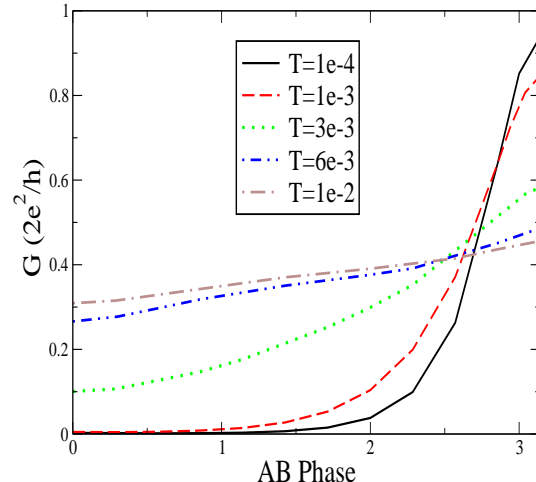


FIG. 5: The conductance as function of the AB phase  $\alpha = 2\pi\Phi/\Phi_0$  for various values of the temperature, for  $L = 403$  ( $n_l = n_r = 101$ ,  $n_0 = 203$ ). The other parameters are unchanged. The dot is in the Kondo regime.

### C. SBMFT results for the conductance through the small ABI

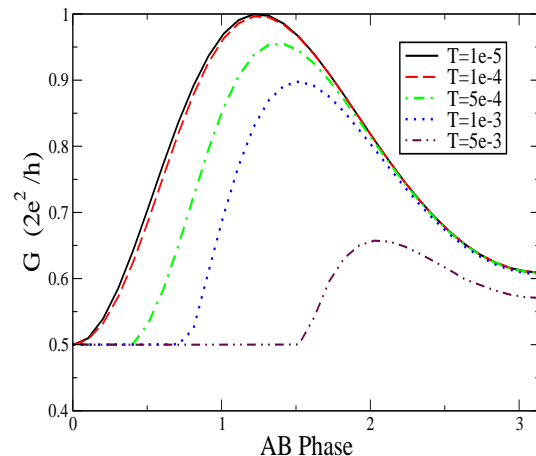


FIG. 6: The conductance of the smallest ABI configuration, as function of the AB phase  $\alpha = 2\pi\Phi/\Phi_0$  for various values of the temperature.

It is interesting to use the slave-boson technique to study the small ABI configuration, introduced in Sec. II B 2 above. Since within the SBMFT one effectively deals with a non-interacting system, the conductance is given, via the Landauer formula, by the transmission [with the various dot parameters being computed self-consistently from the SBMFT Eqs. (30)].



In the case of the small configuration, it is easy to obtain an explicit expression for the energy-dependent transmission coefficient,  $\mathcal{T}(\omega)$ ,

$$\mathcal{T}(\omega) = \frac{4(1 - \frac{\omega^2}{4J^2})}{J^2} \left| g_{00}(\omega) i_\ell i_r \left( 1 + \Sigma_f^R(\omega) G_f^R(\omega) \right) + G_f^R(\omega) b_0^2 j_\ell j_r e^{-i\alpha} \left( 1 + g_L(\omega) g_{00}(\omega) (i_\ell^2 + i_r^2) \right) \right|^2. \quad (32)$$

Here, the self-energy  $\Sigma_f^R$  is given by multiplying the terms of Eq. (17) by  $b_0^2$ . Note that  $\mathcal{T}(\omega)$  is even in  $\alpha$ , and hence satisfies the Onsager relations. This can be seen by factoring out from both members in  $|\dots|^2$  of Eq. (32) the product  $G_f^R g_{00}$ . The remaining terms are real except for the factor  $e^{-i\alpha}$ .

The conductance through the small ABI as function of the AB phase  $\alpha$ , at various temperatures, is depicted in Fig. 6, for the same parameters as used in calculating the Kondo temperature (see Fig. 3). At low temperatures,  $T \leq 10^{-4}$ , the curve is smooth. It corresponds to the low temperature regime  $T \ll T_K(\alpha)$  in which the spin impurity is well screened at all values of the flux (the so-called unitary limit). At higher temperatures there appear the plateau-like features around  $\alpha = 0$ . These values of the flux correspond to the lowest Kondo temperatures (see Fig. 3), where the dot has a small transmission for  $T \gg T_K(\alpha)$ . It is remarkable that even this small ABI configuration already displays the main features associated with the flux-dependent Kondo temperature. Note that the plateaus appear here at the smallest values of the conductance (as opposed to the previous case, see Fig. 4). This feature simply reflects a non-interacting interference effect that depends on the specific choice of parameters which determine the detailed dependence of the Kondo temperature on the AB flux.

#### IV. THE OPEN ABI

As is mentioned in the Introduction, there is much interest in the complex transmission amplitude,  $t_{QD} = |t_{QD}| e^{i\varphi_{QD}}$ , of a quantum dot, particularly in the Kondo regime. While  $|t_{QD}|$  can be inferred from the conductance of the quantum dot, when coupled to two leads, this is not the case with the phase shift  $\varphi_{QD}$ . It has been conjectured that open ABI's, under certain conditions, will mimic the two-slit limit. Has it been the case, the total transmission amplitude of the interferometer threaded by an AB flux would have read  $t_{ABI} \propto t_{QD} e^{i\alpha} + t_B$ , where  $t_B$  is the transmission amplitude of the other arm of the ring. Then, by varying the quantum dot properties (for example, the gate voltage on it, which in our model is  $\epsilon_d$ ), one would have been able to record the phase shift  $\varphi_{QD}$  by monitoring the variations of the conductance (which is determined by  $|t_{ABI}|^2$ ) with the AB flux.<sup>9</sup> Unfortunately, there are several caveats in this attractive scenario. Firstly, the open ABI has to obey rather stringent conditions in order to be in the two-slit limit.<sup>14,15</sup> Secondly, when the quantum dot is placed on the interferometer, its properties are in general changed, because of its coupling to the mesoscopic ring, and due to the presence of the AB flux. In the following, we do not

attempt to search the parameter space in order to find the regions where the open ABI is in the two-slit limit. Rather, we first study the Kondo temperature of an open ABI, and then examine its conductance, as function of the flux, for several values of the gate voltage.

In order to 'open' the ABI in our tight-binding description (see Fig. 1), we attach to each site inside the ring (excluding the sites  $a$  and  $b$  which are already attached to leads) a lead connected in turn to an electronic reservoir, assigning a hopping matrix element  $-J_X$  to its first bond. Such parametrization has been previously used in Ref. 15 to study the conductance through a non-interacting open ABI. Technically, one uses Eq. (13) again, but now Eq. (16) is replaced by a sum of contributions from all the connections to the additional leads.

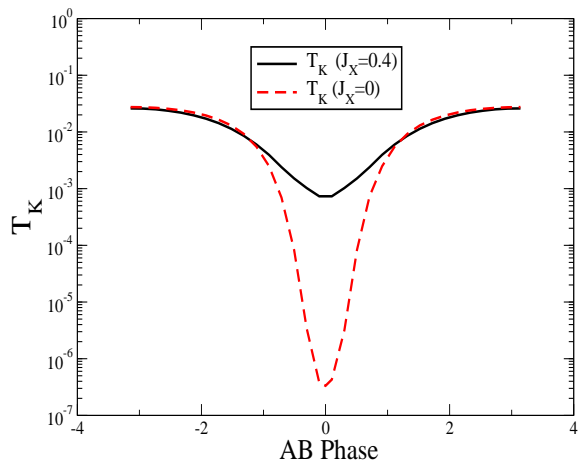


FIG. 7: The Kondo temperature of an open ABI as function of the AB phase for  $J_X = 0.4$  (full line) and  $J_X = 0$  (dashed line). The other parameters used are:  $j_l = j_r = 0.35$ ,  $\epsilon_d = -0.7$ ,  $n_l = n_r = 3$ ,  $n_0 = 5$ ,  $J_L = J_R = 0.6$ .

Figure 7 depicts the dependence of the Kondo temperature of an open ABI on the flux, when the length of the ring is  $L = 11 \ll \xi_K^0 \sim 180$ , taking  $J_X = 0.4$ . For comparison, we have also plotted the Kondo temperature of the closed ABI (for which  $J_X = 0$ ) for the same parameters. We have used the RG definition, Eq. (11), to produce these curves [we have verified that Eq. (9) gives similar results]. It is interesting to note that the bare Kondo temperature pertaining to these parameters is  $T_K^0 \sim 0.011$ . Namely, the Kondo temperature of a dot placed on an ABI is significantly different from the bare one. As can be seen in Fig. 7, the dependence of the Kondo temperature on the AB flux of the open ABI is considerably suppressed as compared to that of the closed one (by more than 3 orders of magnitude!). This implies that the open ABI is less sensitive to finite-size effects than the closed ABI, as could be anticipated: 'Opening' the interferometer smoothes the fine structure of the non-interacting self-energy, and consequently reduces the dependence of the Kondo temperature on the AB phase. Nonetheless, finite-size effects in the open

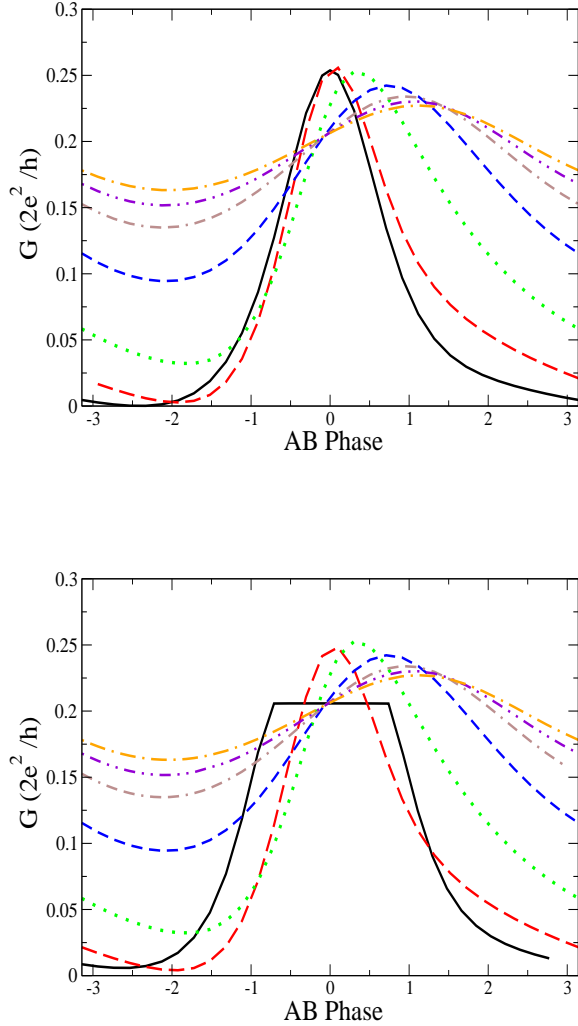


FIG. 8: The conductance of the open ABI as function of the AB phase for  $T = 10^{-4}$  (upper panel) and  $T = 3 \cdot 10^{-3}$  (lower panel) for different values of  $\epsilon_d$ :  $\epsilon_d = -0.7$  (full line),  $\epsilon_d = -0.5$  (long-dashed line),  $\epsilon_d = -0.3$  (dotted line),  $\epsilon_d = 0$  (short-dashed line),  $\epsilon_d = 0.3$  (dashed-dashed-dotted line),  $\epsilon_d = 0.5$  (dotted-dotted-dashed line), and  $\epsilon_d = 0.7$  (long dashed-dotted line).

ABI have not completely disappeared, and the Kondo temperature still varies by a factor  $\sim 50$ .

Next we study the conductance through the open ABI. For such an interferometer, the conductance is no longer an even function of the AB flux. As is discussed above, one is mainly interested in the manner by which the deviation from an even function is modified when the gate voltage, i.e.,  $\epsilon_d$ , is varied. Using the slave-boson technique, we have computed the conductance for several values of this parameter. Figure 8 shows it at two temperatures,  $T = 10^{-4} \ll T_K$  (upper panel) and  $T = 3 \cdot 10^{-3}$  (lower panel). At the lower temperature, the conductance evolves smoothly, and it is possible to extract a phase shift associated with the shift of the maximum of the

conductance upon varying  $\epsilon_d$ . For example, going from the deep Kondo regime ( $\epsilon_d = -0.7$ ,  $n_d \sim 1$ ) to the empty regime ( $n_d \sim 0$ ,  $\epsilon_d = +0.7$ ), this phase shift corresponds here to  $\sim 0.35\pi$ . However, it strongly depends on the other parameters of the ABI (as has been explicitly shown in Ref. 21). At the higher temperature the shift becomes more difficult to read since the maximum around  $\alpha = 0$  for  $\epsilon_d = -0.7$  (deep Kondo regime) is now replaced by a plateau.

## V. CONCLUSION

In this paper we have used the SBMFT to calculate the flux-dependence of both the Kondo temperature of a quantum dot embedded on one branch of an ABI and the conductance through the ABI. One should be aware the SBMFT is not suitable to describe properly the dot charge fluctuations. Therefore, it poorly describes the mixed valence regime and loses its validity in the empty-dot regime. Also, since the slave-boson technique assumes the  $U \rightarrow \infty$  limit, it cannot capture the resonance transmission faithfully, and it may fail in mimicking the details of the experiments. Nonetheless, the above results, particularly in the Kondo regime, demonstrate some qualitative features, which we expect to also arise in more accurate calculations.

Our calculations yields the following conclusions:

- For both the closed and the open ABI, the Kondo temperature of the dot depends on the magnetic flux penetrating the ABI ring. This dependence is very strong (several orders of magnitude) for small ABI's, and weaker for larger ABI's. Thus, the effects of electron interactions strongly depend on the size of the ABI.
- As a result of the above, the flux-dependence of the conductance through the ABI also varies with the size. For small sizes, the system moves from below to above the Kondo temperature as function of the flux, yielding plateaus in the conductance. These plateaus broaden at higher temperature. Unless the temperature is much smaller than the minimal  $T_K(\alpha)$ , one cannot expect to fit the experimental data to any universal function  $G(\alpha)$ .
- The above conclusions apply to both the closed and the open ABI. In particular, they imply that it is very difficult to construct an open ABI that will obey the two-slit formula. In most cases, the shift of the maxima in  $G(\alpha)$  with the gate voltage (as represented by  $\epsilon_d$ ) does *not* reflect the corresponding shift in the transmission phase through the bare dot.<sup>44</sup>

## Acknowledgments

This project was carried out in a center of excellence supported by the ISF under grant No. 1566/04. Work at Argonne is supported by the U.S. Department of Energy under contract W-31-109-Eng-38. Part of the numerical calculations

presented in this paper were performed on the cluster MedEt-Phy (CIMENT, Grenoble).

### APPENDIX A: A GENERAL EXPRESSION FOR THE CURRENT THROUGH AN AHARONOV-BOHM INTERFEROMETER

Here we use the Keldysh technique to derive a general expression for the current through an ABI described by the Hamiltonian Eq. (1) (see also Fig. 1).

We begin by writing down the expressions for the currents  $I_\ell$  and  $I_r$ , entering the ABI from the left lead and from the right lead, respectively,

$$\begin{aligned} I_\ell &= -\frac{e}{h} \int d\omega [\Sigma_{L,\ell}(\omega) G_{n_\ell n_\ell}(\omega) - G_{n_\ell n_\ell}(\omega) \Sigma_{L,\ell}(\omega)]^<, \\ I_r &= -\frac{e}{h} \int d\omega [\Sigma_{L,r}(\omega) G_{n_r n_r}(\omega) - G_{n_r n_r}(\omega) \Sigma_{L,r}(\omega)]^<. \end{aligned} \quad (\text{A1})$$

As in the main text, we denote by  $G$  the Green functions of the full ABI, and by  $g$  the Green functions of the ABI when the dot is disconnected from the ring. In Eq. (A1), the superscript  $<$  denotes the lesser Keldysh Green function, with the lesser Green function of a product being calculated according to the rules derived in Ref. 45.  $\Sigma_L$  is the self-energy due to the semi-infinite leads,

$$[\Sigma_L]_{ij}(\omega) = \delta_{ij}(\delta_{i,-n_\ell} \Sigma_{L,\ell}(\omega) + \delta_{i,n_r} \Sigma_{L,r}(\omega)). \quad (\text{A2})$$

Here  $\Sigma_{L,\ell}$  and  $\Sigma_{L,r}$  are the self-energies resulting from the left and right lead, respectively,

$$\begin{aligned} \Sigma_{L,\ell}(\omega) &= J_L^2 \frac{2}{N} \sum_k \sin^2(k) g_k(\omega), \\ \Sigma_{L,r}(\omega) &= J_R^2 \frac{2}{N} \sum_p \sin^2(p) g_p(\omega), \end{aligned} \quad (\text{A3})$$

where  $g_k(\omega)$  and  $g_p(\omega)$  are the Green functions of the left and right leads, respectively. The two leads are identical, ex-

---

we obtain

$$\begin{aligned} I &\equiv \frac{I_\ell - I_r}{2} \\ &= \frac{e}{h} \int d\omega \left\{ (\Sigma_{L,\ell}^A - \Sigma_{L,\ell}^R) \frac{1}{2} (G_{dd}^< + f_\ell (G_{dd}^R - G_{dd}^A)) |X_{-n_\ell}^R(\alpha)|^2 - (\Sigma_{L,r}^A - \Sigma_{L,r}^R) \frac{1}{2} (G_{dd}^< + f_r (G_{dd}^R - G_{dd}^A)) |X_{n_r}^R(\alpha)|^2 \right. \\ &\quad \left. + (\Sigma_{L,r}^A - \Sigma_{L,r}^R) (\Sigma_{L,\ell}^A - \Sigma_{L,\ell}^R) (f_r - f_\ell) \left[ |g_{-n_\ell n_r}^R|^2 + G_{dd}^R g_{n_r - n_\ell}^A Z_{-n_\ell n_r}^R + G_{dd}^A g_{n_r - n_\ell}^R Z_{-n_\ell n_r}^A \right] \right\}, \end{aligned} \quad (\text{A10})$$

where we have defined

$$Z_{-n_\ell n_r}^R = j_\ell^2 g_{n_r - 1}^R g_{-n_\ell - 1}^R + j_r^2 g_{n_r - 1}^R g_{-n_\ell - 1}^R + j_\ell j_r \cos \alpha (g_{n_r - 1}^R g_{-n_\ell - 1}^R + g_{n_r - 1}^R g_{-n_\ell - 1}^R). \quad (\text{A11})$$

The result (A10) holds in the general interacting case. When there are no electronic interactions on the dot (as also effectively

cept for being connected to electronic reservoirs with different chemical potentials,  $\mu_\ell$  and  $\mu_r$ . Hence,

$$\begin{aligned} \Sigma_{L,\ell}^<(\omega) &= f_\ell(\omega) (\Sigma_{L,\ell}^A(\omega) - \Sigma_{L,\ell}^R(\omega)), \\ \Sigma_{L,r}^<(\omega) &= f_r(\omega) (\Sigma_{L,r}^A(\omega) - \Sigma_{L,r}^R(\omega)), \end{aligned} \quad (\text{A4})$$

with

$$f_\ell(\omega) = \frac{1}{e^{\beta(\omega - \mu_\ell)} + 1}, \quad f_r(\omega) = \frac{1}{e^{\beta(\omega - \mu_r)} + 1}. \quad (\text{A5})$$

The superscripts  $R$  and  $A$  refer to the retarded and advanced Green functions, respectively.

Our aim is to express the current through the interferometer in terms of the dot Green function,  $G_{dd}$ , and the Green functions of the ABI when the dot is disconnected,  $g$ . To this end, we will use the Dyson equation

$$G_{ij} = g_{ii} + X_i(\alpha) G_{dd} \tilde{X}_j(-\alpha), \quad (\text{A6})$$

where

$$\begin{aligned} X_i(\alpha) &= j_\ell e^{-i\alpha/2} g_{i-1} + j_r e^{i\alpha/2} g_{i1}, \\ \tilde{X}_i(-\alpha) &= j_\ell e^{i\alpha/2} g_{-1i} + j_r e^{-i\alpha/2} g_{1i}. \end{aligned} \quad (\text{A7})$$

(Note that while the retarded and advanced Green functions  $g$  are symmetric in the site indices, this is not the case for the Keldysh lesser functions,  $g_{ij}^<$ .) For brevity, we omit here and below the  $\omega$  dependence of the various functions.

Inserting Eq. (A6) into Eqs. (A1) for the left-coming and right-coming currents, we obtain the currents  $I_\ell$  and  $I_r$  in terms of  $G_{dd}^<$  and  $g_{ij}^<$ . The latter is given by

$$g_{ij}^< = g_{i-n_\ell}^R \Sigma_{L,\ell}^< g_{-n_\ell j}^A + g_{in_r}^R \Sigma_{L,r}^< g_{n_r j}^A. \quad (\text{A8})$$

Then, using the relation

$$g_{ij}^R - g_{ij}^A = [g^R (\Sigma_L^R - \Sigma_L^A) g^A]_{ij}, \quad (\text{A9})$$

happens in the slave-boson mean-field approximation), this result can be simplified extensively. In that case,  $G_{dd}^{\leq}$  is known,

$$G_{dd}^{0<} = G_{dd}^{0R} \Sigma_{dd}^{0<} G_{dd}^{0A}, \quad (\text{A12})$$

with

$$\Sigma_{dd}^{0<} = f_r |X_{n_r}^R(\alpha)|^2 (\Sigma_{L,r}^A - \Sigma_{L,r}^R) + f_\ell |X_{-n_\ell}^R(\alpha)|^2 (\Sigma_{L,\ell}^A - \Sigma_{L,\ell}^R). \quad (\text{A13})$$

In addition, when there are no interactions present,

$$G_{dd}^{0R} - G_{dd}^{0A} = G_{dd}^{0R} G_{dd}^{0A} (\Sigma_{dd}^{0R} - \Sigma_{dd}^{0A}), \quad (\text{A14})$$

with

$$\Sigma_{dd}^{0R} - \Sigma_{dd}^{0A} = |X_{-n_\ell}(\alpha)|^2 (\Sigma_{L,\ell}^R - \Sigma_{L,\ell}^A) + |X_{n_r}(\alpha)|^2 (\Sigma_{L,r}^R - \Sigma_{L,r}^A). \quad (\text{A15})$$

Using these expressions in Eq. (A10), we obtain the current through the non-interacting ABI,  $I^0$ ,

$$\begin{aligned} I^0 &= \frac{e}{h} \int d\omega (\Sigma_{L,r}^A - \Sigma_{L,r}^R) (\Sigma_{L,\ell}^A - \Sigma_{L,\ell}^R) (f_r - f_\ell) \left[ |g_{-n_\ell n_r}^R|^2 + |G_{dd}^{0R}|^2 |X_{-n_\ell}^R(\alpha)|^2 |X_{n_r}^R(\alpha)|^2 \right. \\ &\quad \left. + G_{dd}^{0R} g_{n_r - n_\ell}^A Z_{-n_\ell n_r}^R + G_{dd}^{0A} g_{n_r - n_\ell}^R Z_{-n_\ell n_r}^A \right] \\ &= \frac{e}{h} \int d\omega (\Sigma_{L,r}^A - \Sigma_{L,r}^R) (\Sigma_{L,\ell}^A - \Sigma_{L,\ell}^R) (f_r - f_\ell) |G_{-n_\ell n_r}^{0R}|^2, \end{aligned} \quad (\text{A16})$$

where in the last step we have used Eq. (A6). In our tight-binding description of the semi-infinite identical leads,

$$\Sigma_{L,\ell(r)}^A - \Sigma_{L,\ell(r)}^R = i \frac{2J_{L(R)}^2}{J} \sqrt{1 - \left(\frac{\omega}{2J}\right)^2}. \quad (\text{A17})$$

Using this in Eq. (A16), together with  $f_r - f_\ell = (\mu_r - \mu_\ell)(\partial f / \partial \omega)$  leads to the Landauer formula, Eq. (31).

\* On leave from the School of Physics and Astronomy, Raymond and Beverly Sackler Faculty of Exact Sciences, Tel Aviv University, Tel Aviv 69978, Israel.

<sup>1</sup> Y. Imry, *Introduction to Mesoscopic Physics* (Oxford University Press, Oxford 1997; 2nd edition 2002).

<sup>2</sup> R. A. Webb, S. Washburn, C. P. Umbach, and R. B. Laibowitz, *Phys. Rev. Lett.* **54**, 2696 (1985).

<sup>3</sup> M. Büttiker, Y. Imry, and R. Landauer, *Phys. Lett. A* **96**, 3365 (1985).

<sup>4</sup> L. P. Lévy, G. Dolan, J. Dunsmuir, and H. Bouchiat, *Phys. Rev. Lett.* **64**, 2074 (1990); V. Chandrasekhar, R. A. Webb, M. J. Brady, M. B. Ketchen, W. J. Gallagher, and A. Kleinsasser, *Phys. Rev. Lett.* **67**, 3578 (1991); D. Mailly, C. Chapelier, and A. Benoît, *Phys. Rev. Lett.* **70**, 2020 (1993); E. M. Q. Jariwala, P. Mohanty, M. B. Ketchen, and R. A. Webb, *Phys. Rev. Lett.* **86**, 1594 (2001); W. Rabaud, L. Saminadayar, D. Mailly, K. Hasselbach, A. Benoît, and B. Etienne, *Phys. Rev. Lett.* **86**, 3124 (2001); R. Deblock, R. Bel, B. Reulet, H. Bouchiat, and D. Mailly, *Phys. Rev. Lett.* **89**, 206803 (2002).

<sup>5</sup> A. Yacoby, M. Heiblum, D. Mahalu, and H. Shtrikman, *Phys. Rev. Lett.* **74**, 4047 (1995).

<sup>6</sup> R. Schuster, E. Buks, M. Heiblum, D. Mahalu, V. Umansky, and H. Shtrikman, *Nature (London)* **385**, 417 (1997); E. Buks, R. Schuster, M. Heiblum, D. Mahalu, and V. Umansky, *Nature (London)* **391**, 871 (1998).

<sup>7</sup> D. Sprinzak, E. Buks, M. Heiblum, and H. Shtrikman, *Phys. Rev. Lett.* **84**, 5820 (2000).

<sup>8</sup> W. G. van der Wiel, S. De Franceschi, T. Fujisawa, J. M. Elzerman, S. Tarucha, and L. P. Kouwenhoven, *Science* **289**, 2105 (2000).

<sup>9</sup> Y. Ji, M. Heiblum, D. Sprinzak, D. Mahalu, and H. Shtrikman, *Science* **290**, 779 (2000); Y. Ji, M. Heiblum, and H. Shtrikman, *Phys. Rev. Lett.* **88**, 076601 (2002).

<sup>10</sup> K. Kobayashi, H. Aikawa, S. Katsumoto, and Y. Iye, *Phys. Rev. Lett.* **88**, 256806 (2002); K. Kobayashi, H. Aikawa, S. Katsumoto, and Y. Iye, *J. Phys. Soc. Jpn.* **71**, L2094 (2002).

<sup>11</sup> A. W. Holleitner, C. R. Decker, H. Qin, K. Eberl, and R. H. Blick, *Phys. Rev. Lett.* **87**, 256802 (2001).

<sup>12</sup> A. Fuhrer, S. Lüscher, T. Ihn, T. Heinzel, K. Ensslin, W. Wegscheider, and M. Bichler, *Nature (London)* **413**, 822 (2001); U. F. Keyser, C. Fühner, S. Borck, R. J. Haug, M. Bichler, G. Abstreiter, and W. Wegscheider, *Phys. Rev. Lett.* **90**, 196601 (2003); M. Sigrist, A. Fuhrer, T. Ihn, K. Ensslin, S. E. Ulloa, W. Wegscheider, and M. Bichler, *Phys. Rev. Lett.* **93**, 066802 (2004).

<sup>13</sup> G. Hackenbroich, *Phys. Rep.* **343**, 463 (2001).

<sup>14</sup> O. Entin-Wohlman, A. Aharony, Y. Imry, Y. Levinson and A. Schiller, *Phys. Rev. Lett.* **88**, 166801 (2002).

<sup>15</sup> A. Aharony, O. Entin-Wohlman, B. I. Halperin, and Y. Imry, *Phys. Rev. B* **66**, 115311 (2002).

<sup>16</sup> D. Goldhaber-Gordon, H. Shtrikman, D. Mahalu, D. Abusch-

- Magder, U. Meirav, and M. A. Kastner, *Nature (London)* **391**, 156 (1998).
- <sup>17</sup> S. M. Cronewett, T. H. Oosterkamp, and L. P. Kouwenhoven, *Science* **281**, 540 (1998).
- <sup>18</sup> F. Simmel, R. H. Blick, U. P. Kotthaus, W. Wegscheider, and M. Bichler, *Phys. Rev. Lett.* **83**, 804 (1999).
- <sup>19</sup> P. Nozières, *J. Low Temp. Phys.* **17**, 31 (1974).
- <sup>20</sup> U. Gerland, J. von Delft, T. A. Costi, and Y. Oreg, *Phys. Rev. Lett.* **84**, 3710 (2000).
- <sup>21</sup> A. Aharony and O. Entin-Wohlman, *cond-mat/0412068*.
- <sup>22</sup> See e.g. A. Jerez, P. Vitushinsky, and M. Lavagna, *cond-mat/0503229*. We have not been able to compare the results of this paper with those known for the non-interacting limit.
- <sup>23</sup> B. R. Bulka and P. Stefański, *Phys. Rev. Lett.* **86**, 5128 (2001).
- <sup>24</sup> W. Hofstetter, J. König, and H. Schoeller, *Phys. Rev. Lett.* **87**, 156803 (2001).
- <sup>25</sup> J. König and Y. Gefen, *Phys. Rev. Lett.* **86**, 3855 (2001); *Phys. Rev. B* **65**, 045326 (2002).
- <sup>26</sup> O. Entin-Wohlman, Y. Imry, and A. Aharony, *Phys. Rev. B* **70**, 075301 (2004).
- <sup>27</sup> R. López, D. Sánchez, M. Lee, M.-S. Choi, P. Simon, and K. Le Hur, *Phys. Rev. B* **71**, 115312 (2005).
- <sup>28</sup> O. Entin-Wohlman, A. Aharony, and Y. Meir, *Phys. Rev. B* **71**, 035333 (2005).
- <sup>29</sup> W. B. Thimm, J. Kroha, and J. von Delft, *Phys. Rev. Lett.* **82**, 2143 (1999).
- <sup>30</sup> I. Affleck and P. Simon, *Phys. Rev. Lett.* **86**, 2854 (2001); P. Simon and I. Affleck, *Phys. Rev. B* **64**, 085308 (2001).
- <sup>31</sup> H. Hu, G.-M. Zhang, and Yu Lu, *Phys. Rev. Lett.* **86**, 5558 (2001).
- <sup>32</sup> E. Sorensen and I. Affleck, *Phys. Rev. Lett.* **94**, 086601 (2005).
- <sup>33</sup> V. Ferrari, G. Chiappe, E. V. Anda, and M. D. Davidovich, *Phys. Rev. Lett.* **82**, 5088 (1999).
- <sup>34</sup> K. Kang and S-C. Shin, *Phys. Rev. Lett.* **85**, 5619 (2000); K. Kang, S. Y. Cho, J-J. Kim, and S-C. Shin, *Phys. Rev. B* **63**, 113304 (2001).
- <sup>35</sup> H.-P. Eckle, H. Johannesson, and C. A. Stafford, *Phys. Rev. Lett.* **87**, 016602 (2001).
- <sup>36</sup> A. A. Aligia, *Phys. Rev. B* **66**, 165303 (2002).
- <sup>37</sup> P. Simon and I. Affleck, *Phys. Rev. Lett.* **89**, 206602 (2002); *Phys. Rev. B* **68**, 115304 (2003).
- <sup>38</sup> P. S. Cornaglia and C. A. Balseiro, *Phys. Rev. Lett.* **90**, 216801 (2003).
- <sup>39</sup> C. H. Lewenkopf and H. A. Weidenmüller, *Phys. Rev. B* **71**, 121309(R) (2005).
- <sup>40</sup> The non-interacting self-energy of the dot (which determines the Kondo temperature) in this special case is  $\Sigma_{dd}^0(\omega) = 2j_l^2 [\cos^2(\alpha/2)g_1^e(\omega) + \sin^2(\alpha/2)g_1^o(\omega)]$ , where  $g_1^{e/o}$  are the non-interacting Green functions at the extremity of the even/odd lead. In the very long wire limit,  $n_l \gg \xi_K^0 \gg 1$ , one may use a continuum approximation in which the very fast variations of  $g_1^{e/o}(\omega)$  are replaced by their (energy) average values,  $\rho_1^e = -Im(g_1^e)/\pi \approx const.$  and  $\rho_1^o = -Im(g_1^o)/\pi \approx const.$ , and the real part of  $\Sigma_{dd}^0$  is neglected. Then,  $\Sigma_{dd}^0$  becomes phase-independent.
- <sup>41</sup> A. C. Hewson, *The Kondo Problem to Heavy Fermions* (Cambridge University Press, Cambridge, UK, 1997), Chap 7.
- <sup>42</sup> Note that the variations of  $T_K^{SBMFT}$  with the flux, in the case of a large-size ABI, are mainly due to the flux-dependence of  $\Delta$  (the imaginary part of the non-interacting self-energy). The slave boson parameter  $b_0$  is almost constant for the  $L = 403$  ABI, as opposed to the  $L = 21$  one.
- <sup>43</sup> C. Caroli, R. Combescot, P. Nozières, and D. Saint-James, *J. Phys. C* **4**, 916 (1971).
- <sup>44</sup> However, the two-slit formula poses several consistency checks, which can be tested on the measured data [A. Aharony, O. Entin-Wohlman, and Y. Imry, *Physica E* (in press); *cond-mat/0412027*].
- <sup>45</sup> D. C. Langreth, in *Linear and Nonlinear Electron Transport in Solids*, Vol. 17 of *Nato Advanced Study Institute, Series B: Physics*, edited by J. T. Devreese and V. E. Van Doren (Plenum, New York, 1976).